Synthesis and study of nickel sulfide nanoparticles and nanostructures for energy storage device applications

Mahesh M. Kamble[1], Bharat R. Bade[2], Avinash V. Rokade[2], Vaishali S. Waman[3], Sachin V. Bangale[4], Sandesh R. Jadkar[2]

[1] PDEA'S Anantrao Pawar College, Pirangut, Mulshi, Pune 412115 India

[2] Department of Physics, Savitribai Phule Pune University, Pune 411007 India

[3] P. E. S. Modern College of Arts, Science and Commerce, Shivajinagar, Pune 411005 India

[4] Chemical Research Lab, UG and PG Department of Chemistry, G. M. Vedak College of Science, Tala-Raigad, 402111 India

Corresponding author: Mahesh M. Kamble, mmkamble14@gmail.com

ABSTRACT Nickel sulfide (NiS) nanostructures were synthesized by simple and low-cost hot injection method (HIM). The effects of sulfur concentration on the compositional, morphological, optical and structural properties of NiS nanoparticles were investigated in detail. The X-ray diffraction pattern confirms the formation of NiS nanoparticles without any impurities. The Raman spectra show the presence of NiS active modes in the synthesized material prepared at different sulphur concentration. The electrochemical performance of the synthesized NiS powder was estimated through cyclic voltammetry, galvanostatic charge-discharge, and electrochemical impedance spectroscopy in KOH electrolyte. The specific capacitance (CS) of the NiS powder electrode was measured with the three-electrode method, and it confirms the maximum CS of 315.8 F/g at a scan rate of 5 mVs^{-1}. The calculated value of energy density and power density of the NiS powder electrode is 3.324 WhKg^{-1} and 199 WKg^{-1} respectively at a lower current density. Present study provides a simple and low-cost HIM is capable for controlling the structural, optical, and morphological properties of nickel sulfide series, which would be of great potential for the synthesis of other metal sulfides.

KEYWORDS nickel sulfide, nanoparticles, nanostructures, electrochemical measurements, supercapacitor, hot injection method

1. Introduction

The development of efficient, clean and high-performance energy storage systems is a basic need of the community. There are different energy storage systems like batteries, fuel cells, supercapacitors etc. among them supercapacitors have attracted much attention due to their excellent electrochemical performance. The supercapacitors are significant part of energy storage systems due to its outstanding properties like high power densities, fast charge-discharge rates, relatively low costs, long operational life, and environmental friendliness. Moreover, the supercapacitor possesses more energy and power density as compared with rechargeable lithium batteries. Supercapacitors have been extensively used in many fields including electronics, defense, transportation, communications etc. To develop high-performance supercapacitors, good choice of electrode materials is important. It is the key parameter for the capacitance performance in the energy storage device applications [1]. So, the synthesis of novel materials using low-cost techniques along with higher specific capacitance and power densities is a challenge for many researchers. Hence, there is a strong inspiration to search inexpensive and promising alternative electrode materials for supercapacitor applications. The metal oxides/metal hydroxides, conductive polymers, carbonaceous materials etc. have been used to construct supercapacitor electrodes [2–4]. The high resistivity of metal oxides affects the storing capacities and cyclic performance. Various conducting polymers have been utilized for the fabrication of supercapacitor electrodes but they have poor cyclic stability. Nowadays, transition metal sulfides like NiS, CoS, CuS, ZnS etc. have attracted more attention in energy applications because of their excellent properties such as high electrical conductivity, better electrochemical stability, eco-friendly nature, and low-cost [5].

Among all the existing electrode materials, transition metal sulfides have been studied more due to their excellent electrical properties and capacity to exhibit various redox states [6–9]. Among the transition metal sulfides, NiS has made more interest due to its superior properties such as high electron conduction, low cost, rich chemical composition, natural

abundance, environmental benignity, ease of fabrication and low toxicity [10–13]. Thus, due to its outstanding properties, nickel sulfide has been widely used in rechargeable lithium batteries, infrared detectors, hydro sulfurization catalysis, photoconductive material, dye-synthesized solar cells, solar energy storages etc. [14]. There are several methods used for the synthesis of nickel sulfide which includes high temperature solid state and vapour phase reaction [15], hydrothermal [16], solvothermal [17], microwave radiation [18], sonochemical method [19] etc. In solvothermal and vapor phase, process requires high temperature; in this method, it is difficult to get a controlled NiS phases. In the hydrothermal method, other phases are created in the synthesized material. In this work, we have synthesized device quality NiS nanoparticles at different sulphur concentrations by using a locally fabricated hot injection system, particulars of which have been explained elsewhere [20].

2. Experimental

2.1. Materials

Oleylamine (OAm, 70 %), nickel nitrate hexahydrate ($Ni(NO_3)_2 \cdot 6H_2O$, 99.999 %), sulphur powder (S, 99.98 %), acetone (99.9 %), toluene (99 %) and isopropanol (IPA, 99.5 %) were used for NiS synthesis with the purity level mentioned in parenthesis. The chemicals mentioned above used for the synthesis of nickel sulfide were procured from Sigma-Aldrich and used without further filtering and processing.

2.2. Synthesis of high-quality NiS nanoparticles

The colloidal NiS nanoparticles were synthesized by the hot injection method. The oleylamine is used as a solvent, surfactant and capping ligand. In a 100 mL three naked glass flask, 0.2 molar nickel nitrate hexahydrate [$Ni(NO_3)_2 \cdot 6H_2O$] and 15 mL of oleylamine were added. The one end of three naked flasks is connected to alternately vacuum and argon gas balloon, the other end is used for injecting sulfur and the third end is used for thermocouple to measure reaction temperature. The resultant solution was constantly stirred using a magnetic stirrer and heated to a steady temperature of 140 °C in an alternate vacuum and argon gas environment to remove moisture and air from the reaction zone. Once the Ni-Oleyamine complex turned into the light brown-black solution, the reaction temperature was raised to 210 °C and kept constant for an hour, as the required crystal size and morphology depend on the temperature of the reaction.

Meanwhile, another solution was prepared, for which one molar sulphur powder was mixed with 5 mL oleylamine, which is named as S-Oleyamine solution. The S-Oleyamine solution was stirred and heated at 80 °C for 45 minutes. The resulting heated S-Oleyamine solution was rapidly injected into the preheated Ni-Oleylamine complex solution. The resulting mixture was heated to 210 °C for 30 minutes, getting a homogeneous blackish solution. All reactions were carried out in alternate vacuum and argon gas atmospheres. After that the three-necked glass flask was kept in a cold water bath to cool the reaction mixture. The same experiments were repeated in this set for 2 and 3 molar sulphur concentrations. The 1, 2 and 3 molar sulphur concentration means 1, 2 and 3 molar sulphur powder was mixed with 5 mL oleylamine.

The NiS nanoparticles are dispersible in organic solvents such as toluene and isopropanol, so 5 mL of toluene and 40 mL of isopropanol were added in resulting mixture to precipitate the NiS nanoparticles. The precipitate was recovered by centrifugation at 3000 rpm to yield colloidal black NiS nanoparticles. The isopropanol and toluene were used to remove polar and non-polar impurities respectively. The colloidal NiS nanoparticles were annealed at a temperature of 350 °C for one hour. Finally, NiS powders were taken out for characterization and confirmation. Fig. 1 shows the schematic for the synthesis of NiS powder.

2.3. Characterization

The structural properties of NiS nanoparticles were confirmed from the XRD pattern recorded on a Bruker D8 advanced diffraction meter with CuKα radiation at a wavelength of $\lambda = 1.54$ Å. The optical properties of synthesized materials were confirmed from a UV-Vis spectrophotometer (Jasco, model V-670) in the wavelength range of $200 - 1400$ nm. Scanning Electron Microscopy (SEM) (JEOL-6360-LA instrument) is used for the study of surface morphology. The elemental compositions were confirmed from Energy Dispersive X-ray Analysis (EDAX). The Raman Spectroscopy is used to identify active modes of Nis nanoparticles and it is recorded with a Renishaw Raman Microscope with argon laser at 532 nm in the $200 - 900$ cm^{-1} range. The bonding configurations in the materials were confirmed from Fourier Transform Infrared Spectroscopy (FTIR) (Jasco, 6100-type A) in the range $400 - 4000$ cm^{-1}. The electrochemical performance of synthesized NiS powder electrode was estimated by cyclic voltammetry, galvanostatic charge-discharge and electrochemical impedance spectroscopy.

3. Results and discussion

3.1. XRD Analysis

The X-ray diffraction patterns of the nickel sulfide nanoparticles synthesized using the hot injection method at various sulphur concentrations are shown in Fig. 2. The crystallographic information of NiS nanoparticles was confirmed by the XRD analysis. The XRD pattern of the synthesized material was recorded in the range of diffraction angle from 15 to 80°.
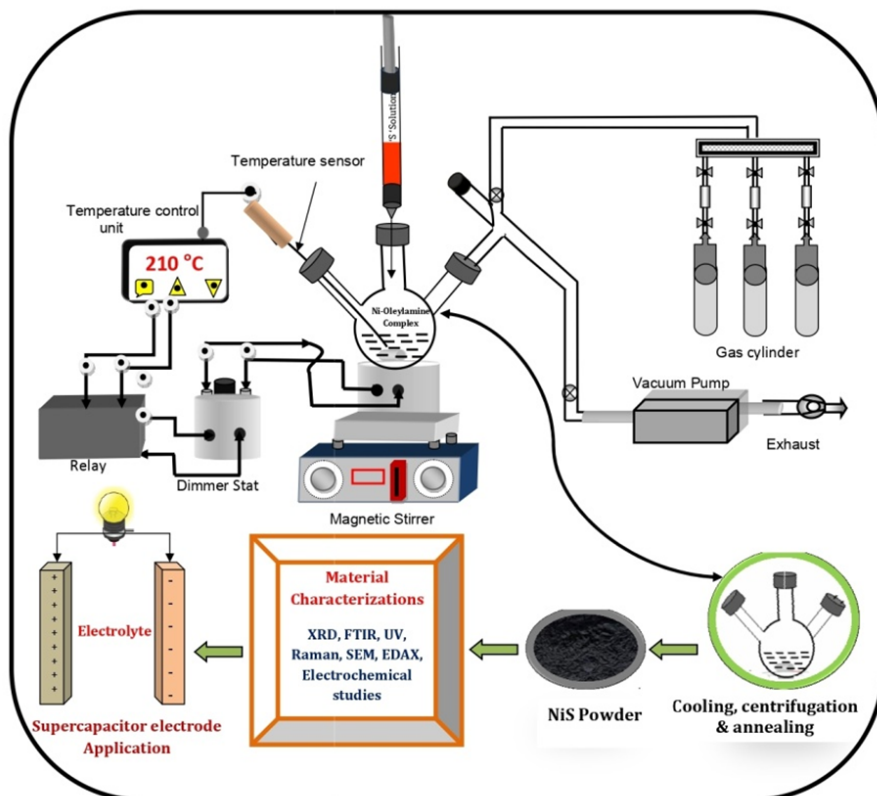
FIG. 1. Schematic for the synthesis of NiS powder

The XRD pattern of NiS synthesized at 2 molar sulphur concentration shows major diffraction peaks at two theta equal to 30.24, 34.54, 45.74, 53.57, 60.80, 62.68, 65.31, 70.64, and 73.10° which is perfectly indexed to the NiS reflections of (100), (101), (102), (110), (103), (200), (201), (004), and (202) crystal planes respectively. The observed well-defined diffraction peaks of NiS nanoparticles are well indexed to the hexagonal phase of NiS with space group P6$_3$/mmc (JCPDS No.: 10-075-0613) [21]. No other peaks were observed in the XRD pattern, indicating that pure NiS nanoparticles were successfully synthesized. The NiS nanoparticles synthesized at 1 molar sulphur concentration confirm a major diffraction peak of 100 plane whereas NiS nanoparticles synthesized at 3 molar sulphur concentrations shows 100, 101, 102 and 110 diffraction peaks. The NiS nanoparticles synthesized at 2 molar sulphur concentration show well crystalline nature as compared with the other two samples. Thus, the sulphur concentrations play an important role in the synthesis of well crystalline NiS nanoparticles. The intense and sharp diffraction peaks suggest that the synthesized NiS is well crystalline. The average crystalline size of synthesized NiS materials has been calculated from the Debye–Scherrer formula

$$d_{\text{x-ray}} = \frac{0.9\lambda}{\beta \cos \theta}, \tag{1}$$

where $d_{\text{x-ray}}$ is the crystalline size, λ is the wavelength of X-ray, β is full width half maxima (FWHM) and θ is the diffraction angle. The average crystalline size of synthesized NiS nanoparticles synthesized at 2 molar sulphur concentrations is found to be 58 nm. The lattice constants and average crystalline size of NiS nanoparticles synthesized at different sulphur concentrations are listed in Table 1. The observed and calculated XRD parameters of the NiS sample are listed in Table 2.

TABLE 1. Lattice constants and average crystalline size of NiS nanoparticles synthesized at different sulphur concentration

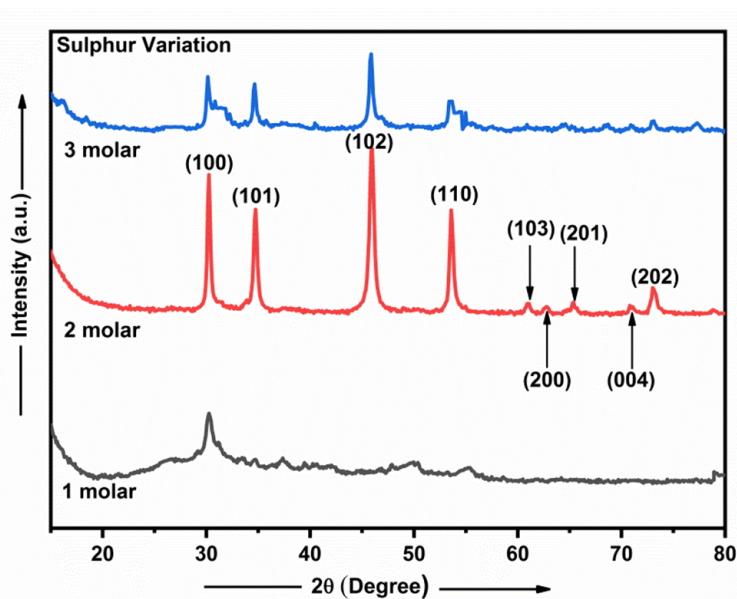| Sulphur concentration (Mole)	Lattice constant (Å)		Average crystalline size (nm)
	a	c	
1	3.4152	5.2264	42
2	3.4197	5.3174	58
3	3.4086	5.3268	46

FIG. 2. XRD pattern of NiS nanoparticles synthesized at different sulphur concentration

TABLE 2. Indexed X-ray diffraction pattern of NiS nanoparticles

Sr. No.	2θ	Interplaner spacing (observed) Å	Interplaner Spacing (calculated) Å	[hkl]
1	30.14	2.9618	2.9615	100
2	34.54	2.5854	2.5936	101
3	45.74	1.9749	1.9812	102
4	53.57	1.7100	1.7086	110
5	60.80	1.5172	1.5216	103
6	62.68	1.4809	1.4804	200
7	65.31	1.4262	1.4270	201
8	70.64	1.3250	1.3318	004
9	73.10	1.2927	1.2929	202

3.2. Raman analysis

The Raman spectrum of NiS nanoparticles synthesized at different sulphur concentrations is shown in Fig. 3. Raman bands observed at 181, 345 and 533 cm^{-1} indicates the formation of NiS [22]. However, not all vibrational modes of NiS have been observed, which could affect the effect of quantum confinement on the vibrational modes of NiS nanoparticles [23]. The decrease in the sharpness of the peak is related to a reduction of the volume fraction of crystallites in the material [24]. Fig. 3 shows that material synthesized at 2 molar suphur concentration is more crystalline as compared with the other two samples.

3.3. Optical properties

The optical properties of NiS nanoparticles synthesized using the hot injection method at different sulphur concentrations are shown in Fig. 4. For NiS nanoparticles, the UV-Vis absorption spectra show peaks at 285, 287 and 290 nm for the sample synthesized at 1, 2 and 3 molar sulphur concentrations, respectively. These peaks can be attributed to the band edge absorption of NiS nanoparticles. The absorption spectrum shows a blue shift compared to the NiS bulk (295 nm) [25], due to the small size of the particles [26].

The optical band gap of NiS nanoparticles is calculated using Tauc's relation [27]
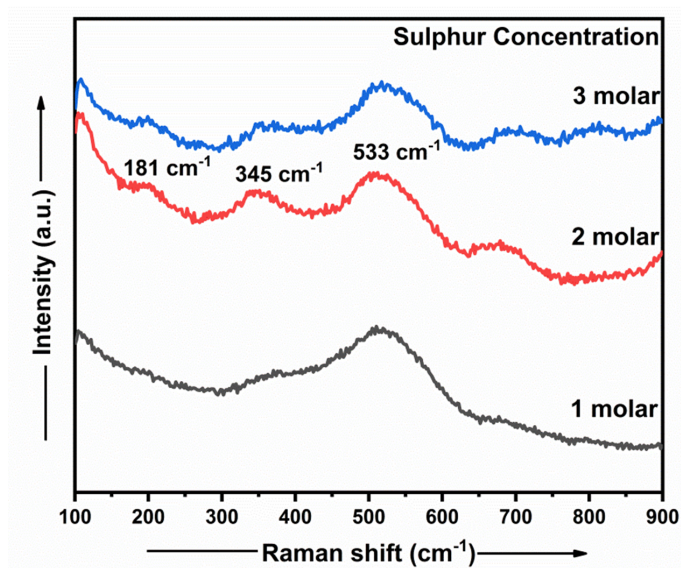
$$\alpha h\upsilon = k(h\upsilon - E_g)^n, \tag{2}$$

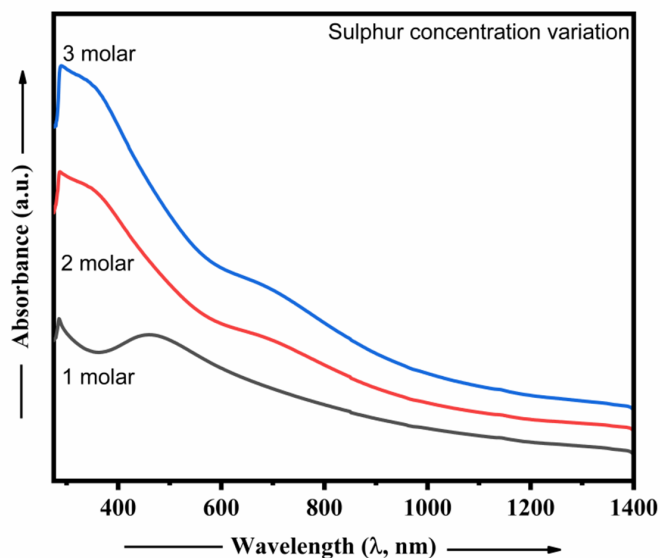FIG. 3. Raman spectra of NiS nanoparticles synthesized at different sulphur concentration

FIG. 4. Absorbance spectra of NiS nanoparticles

where, α is the absorption coefficient, υ is the frequency, h is Planck's constant, k and n are constants. The plots of $(\alpha h \upsilon)^2$ Vs. $h\upsilon$ for NiS nanoparticles are shown in Fig. 5. The optical band gap energy is calculated by extrapolating the linear portion of the curve to the energy axis. The band gap energy of NiS nanoparticles synthesized at 1, 2 and 3 molar sulphur concentration was found to be 1.9, 1.98 and 1.81 eV, respectively. We have observed that the band gap energy of the synthesized material is higher than its bulk [28].

3.4. Morphological properties of NiS nanoparticles

The surface morphological features of NiS nanostructures were studied by using SEM. The SEM images of NiS nanostructures synthesized at different sulphur concentrations by the hot injection method are shown in Fig. 6. From the SEM images agglomeration of nanoparticles with irregular shapes were observed. The SEM images of NiS nanostructures synthesized at different sulphur concentrations show porous in nature.

The EDAX spectra were used for knowing the atomic % of the elements in the synthesized samples. The EDAX spectrum shows the presence of nickel and sulphur in the synthesized material. Table 3 shows the elements in atomic % of the samples synthesized at different sulphur concentrations. From Table 3, it is clear that as sulphur concentration increases atomic % of sulphur enhances whereas the atomic % of nickel reduces in the synthesized material and it is equivalent to the initial mixture used for the synthesis. Fig. 7 shows the EDAX spectra of the NiS nanostructures synthesized at different sulphur concentrations.
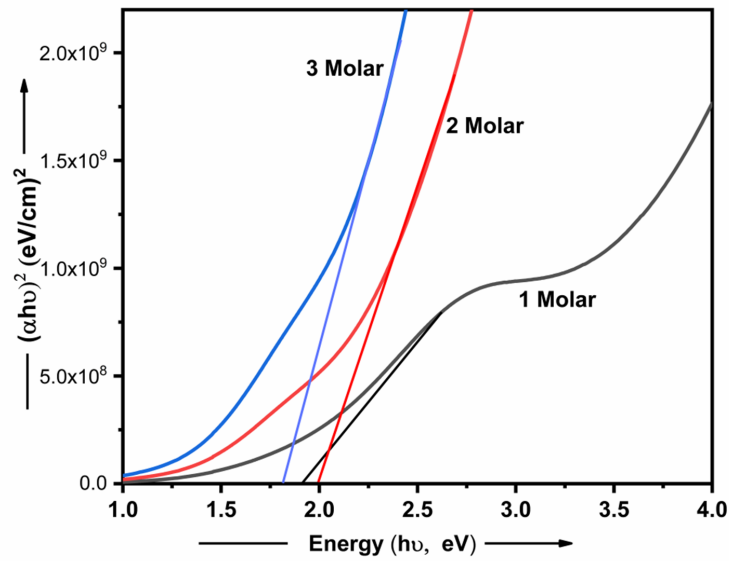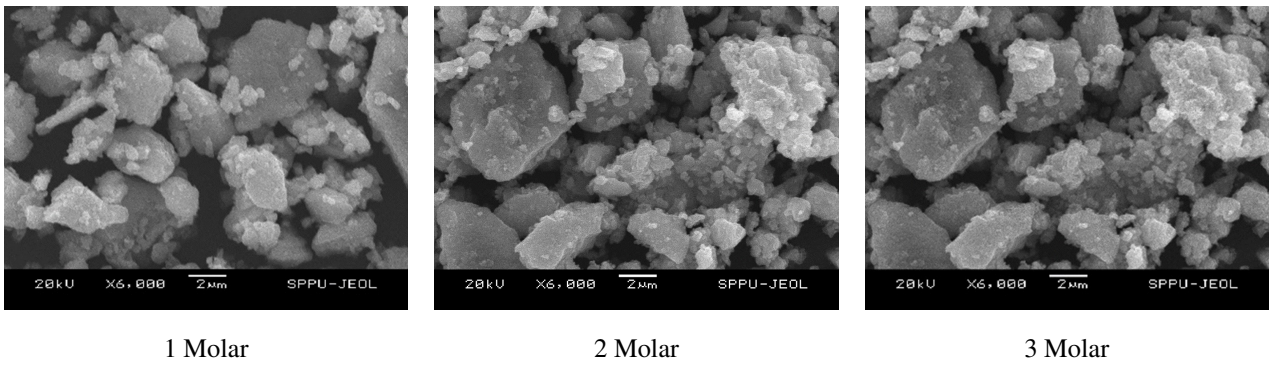
FIG. 5. Tauc's plot of NiS nanoparticles

1 Molar   2 Molar   3 Molar

FIG. 6. SEM images of NiS nanostructures synthesized at different sulphur concentration

TABLE 3. The elemental compositions of NiS nanstructures synthesized at different sulphur concentrations in terms of atomic %

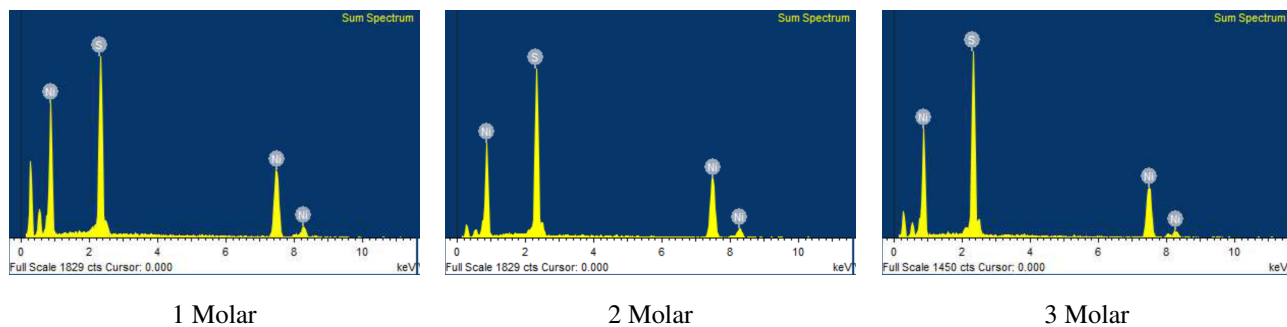| Sulphur concentrations	Elements	Atomic %
1 molar	Sulphur	54.41
	Nickel	45.59
2 molar	Sulphur	56.10
	Nickel	43.90
3 molar	Sulphur	60.72
	Nickel	39.28

| 1 Molar | 2 Molar | 3 Molar |

FIG. 7. EDAX spectra of NiS nanostructures synthesized at different sulphur concentration

3.5. FTIR analysis

The synthesized NiS nanoparticles were further examined by FTIR spectroscopy. Fig. 8 shows the FTIR spectra of nickel sulphide nanoparticles synthesized at different sulphur concentrations by the hot injection system. The absorption bands observed nearly at 640 and 960 cm^{-1} are associated to the symmetrical and asymmetrical stretching of the nickel-sulphur (Ni–S) band in NiS particles. The bending vibrations of the sulfonated group were confirmed from the peak observed at 1140 cm^{-1} [29]. The peak observed nearly at 652 cm^{-1} is related to Ni–S–Ni bending vibration mode and the absorption band nearly at 503 cm^{-1} is due to Ni–S bending vibration [30]. The very small bands appeared in the FTIR spectra nearly at 2920 cm^{-1} is due to the bending vibration of H$_2$O molecules. The IR bands appeared nearly at 1464 and 3005 cm^{-1}, indicating amine ligand is bound to the nanoparticles [31]. Thus, from FTIR spectra, it is clear that no additional IR vibrational peaks were observed indicates the high purity of synthesized powder.
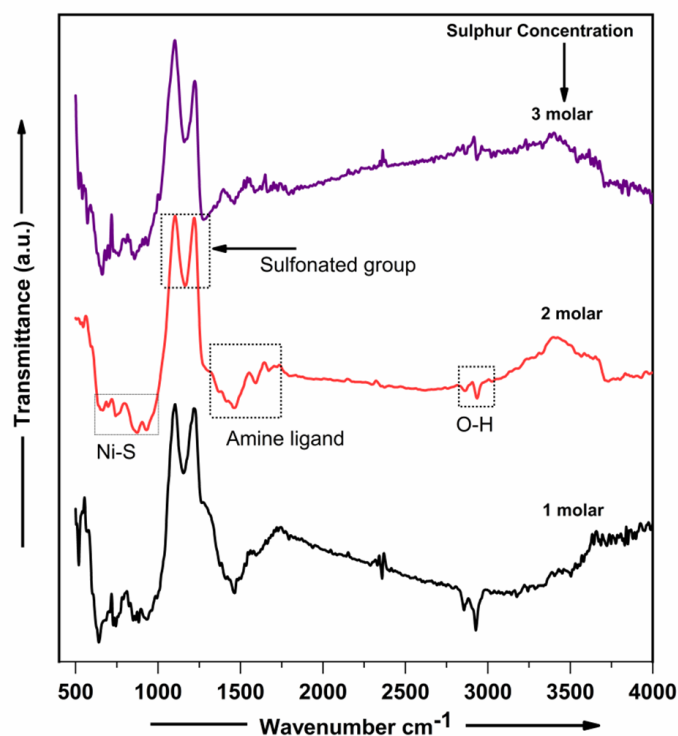

FIG. 8. FTIR spectra of NiS nanoparticles synthesized at different sulphur concentration

3.6. Electrochemical studies

3.6.1. Electrode preparation. The electrode was prepared by mixing 80 wt% nanocrystalline NiS powder as an active material, 10 wt% activated carbon as a conducting additive and 10 wt% Polyvinyl difluoride (PVDF) as a binder in N-Methyl Pyrrolidone (NMP) solvent. The slurry was grinded adequately in the mortar pestle to get a homogeneous mixture, after that it was coated on a carbon paper substrate (1 cm × 1 cm area) using the doctor blade technique. This technique was firstly developed by Glen Howatt for the fabrication of thin sheets of ceramic capacitors [32]. In this technique,

material to be deposited (slury) is fixed between the blade and substrate. During the fabrication of the film, there is a constant relative movement between the blade and substrate in which slurry uniformly spreads on the substrate. The doctor blade technique is used for large area film fabrication. It is technologically simple and low-cost. Despite these nearly 100 % materials are utilized for film fabrication and hence the small quantity of material is sufficient to form the well defined thickness of film [33]. The mass of the material loaded on the substrate was calculated via the weight difference method. The fabricated electrodes were dried at 150 °C for overnight inside a hot air oven to remove solvent and were used as a working electrode for further electrochemical analysis.

3.6.2. Electrochemical studies. Herein, the cyclic voltammetry (CV), galvanostatic charge-discharge (GCD), and electrochemical impedance spectroscopy (EIS) measurements of NiS powder electrode synthesized at 2 molar sulphur concentration was carried out to examine and evaluate supercapacitive performance using a potentiostat (Metrohm Autolab: PGSTAT302N model). The measurement system consists of a cell in three-electrode configurations adopting the carbon paper coated with active material as a working electrode, Platinum foil as a counter and Hg/HgO as a reference electrode. All measurements were evaluated in aqueous solution of 2 M KOH. The EIS measurements were investigated using the same potentiostat with three-electrode cell configurations under open circuit voltage with amplitude of 10 mV between applied frequency sweeps from 1 MHz to 0.1 Hz.

3.6.3. Cyclic coltammetry (CV). The specific capacitance (CS in F/g) and energy density (E) of the NiS powder electrode was calculated from cyclic voltammetry (CV) measurements using equations (3) and (4):

$$C_p = \frac{1}{ms\Delta V} \int I(V)dV, \tag{3}$$

$$E_{cv} = \frac{1}{2}C_p \cdot \Delta V^2, \tag{4}$$

where m is the mass of active materials loaded on working electrode (in gm), I is the response current (in A), $\int I(V)dV$ is area under the current-voltage (CV) curve, s is the scan rate (in mVs^{-1}) and ΔV is operating potential windows (in volt).

CV measurements of the synthesized NiS powder electrode were carried out with potential range from 0.0 to 0.5 V at different scan rates of 5, 10, 20, 50 and 100 mV/s is presented in Fig. 9. The material synthesized at 2 molar sulphur concentration shows better electrochemical performance compared with the others. As the scan rate increases the shapes of CV graphs remain almost the same showing the excellent electrode capabilities and ideal supercapacitor nature [34]. The CV measurements show that as the scan rate increases, the area of the CV curve enhances denoting the behavior of an ideal capacitor. The highest specific capacitance value is 315.8 F/gm for 2 molar sulphur concentrations due to the great synergistic interaction between nickel and sulphur. The maximum value of specific capacitance may be due to the porous nature of the material as examined from SEM in which superior exposure of active sites and easier electrolyte access [35]. As the scan rate decreases the specific capacitance enhances, and the maximum capacitance was observed at lowest scan rate 5 mVs^{-1}. The calculated energy density values from CV graph is 6.99 WhKg^{-1}. Moreover, to illustrate the importance of this work, we have compared the present study with the earlier work reported in literature by considering different materials for supercapacitor electrode applications.

TABLE 4. Comparisons of the earlier studies reported for supercapacitor electrode applications

| Sr. no.	Material	Method of synthesis	Electrolyte	Potential Window V	Specific capacitance (Fg^{-1})	Reference
1	CoS	Chemical bath deposition	Ethanol	−0.4 to 0.6	41.36	[36]
2	Nickel sulfide/ reduced graphene oxide	Solution combustion Method	KOH	0.0 to 0.4	305	[37]
3	NiFe$_2$O$_4$	Chemical oxidation	KOH	0.0 to 0.45	266	[38]
4	Mg$_{0.1}$Mn$_{0.9}$Fe$_2$O$_4$	Solvothermal reflux	KOH	0.0 to 0.6	226.4	[39]
5	NiS	Hot injection method	KOH	0.0 to 0.5	315.8	Present work
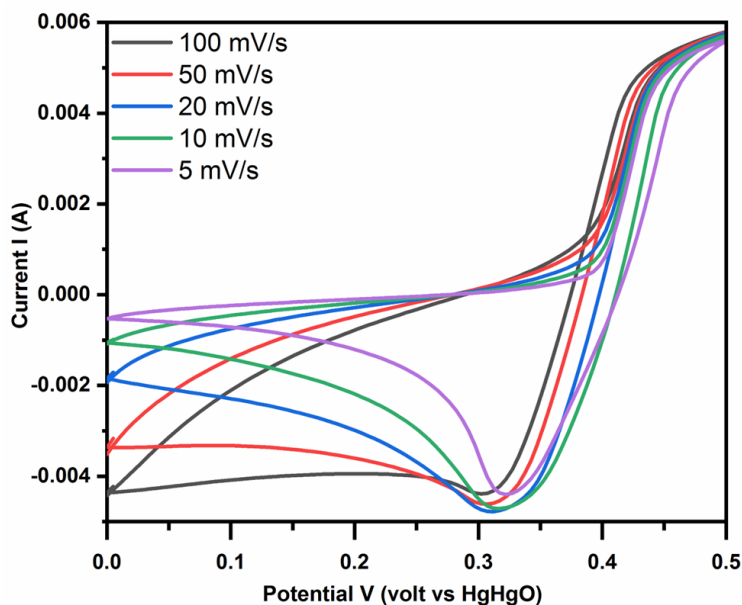
FIG. 9. CV measurements of the synthesized NiS powder electrode recorded in the voltage range of 0 to 0.5 V at different scan rates

3.6.4. Galvanostatic charge-discharge (GCD). The GCD study of the NiS powder electrode was carried out at different current densities 1.0, 1.5 and 2.0 A/g within the potential window 0 to 0.4 V in 2 M KOH electrolyte. Fig. 10 shows the GCD curves of NiS powder electrode at different current densities. The specific capacitance CS (Fg^{-1}), energy density E ($WhKg^{-1}$) and power density P (WKg^{-1}) can also be calculated from the galvanostatic charge-discharge plot using the following equation.

$$C_s = \frac{I \cdot t_d}{m \cdot \Delta V}, \tag{5}$$

$$E = \frac{1}{2}C_s \cdot \Delta V^2, \tag{6}$$

$$P = \frac{E}{t_d}, \tag{7}$$

where I is the response current (A), m is the mass of active material (kg), ΔV is the potential window (V), and t_d is the discharge time (h). The calculated value of energy density is 3.324 $WhKg^{-1}$ and power density 199 Wkg^{-1} for lower current density.
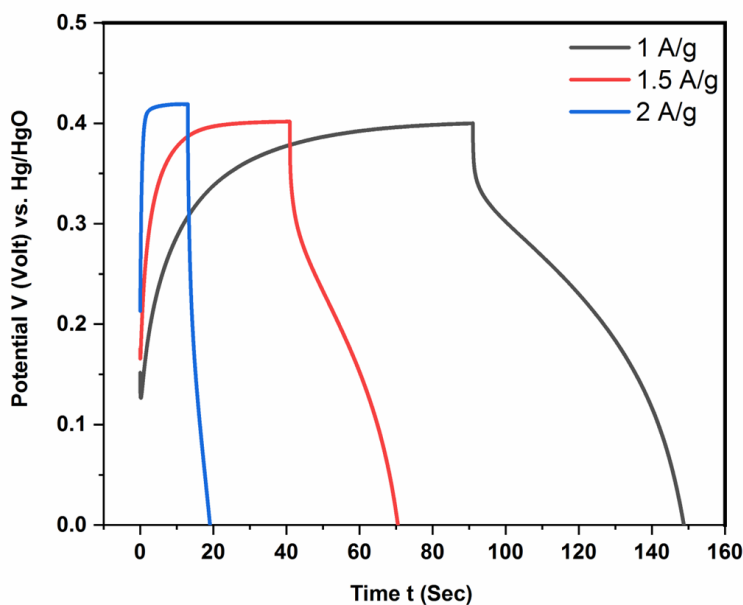

FIG. 10. Charging-discharging performance of NiS electrode at different current densities

The Nyquist plot of the NiS powder electrode synthesized at 2 molar sulphur concentrations was measured in the frequency range from 1 Mhz to 0.1 Hz as presented in Fig. 11. The nearly vertical line in the Nyquist plot shows the ideal supercapacitor nature and the diameter of the small semicircle in high-frequency range represents the interfacial charge transfer resistance (R_{ct}) between the electrolyte and electrode. The intersecting point with the real axis in the high-frequency region represents the internal resistance (R_s) of the electrode material (including ionic resistance, inherent resistance of material and contact resistance of electrode material and electrolyte). The Nyquist plot is fitted to an equivalent electronic circuit, as shown in the inset of the Fig. 11. The values of R_s and R_{ct} are 9 and 7.3 ohm. The Warburg resistance was due to the diffusion of the electrolyte in the bulk of the electrode. The small semicircle arc in high-frequency region indicates good electrical conductivity and low charge transfer resistance of the electrode materials. Thus, the Nyquist plot shows NiS powder synthesized at 2 molar sulphur concentration shows good electrical conductance with high specific capacitance.
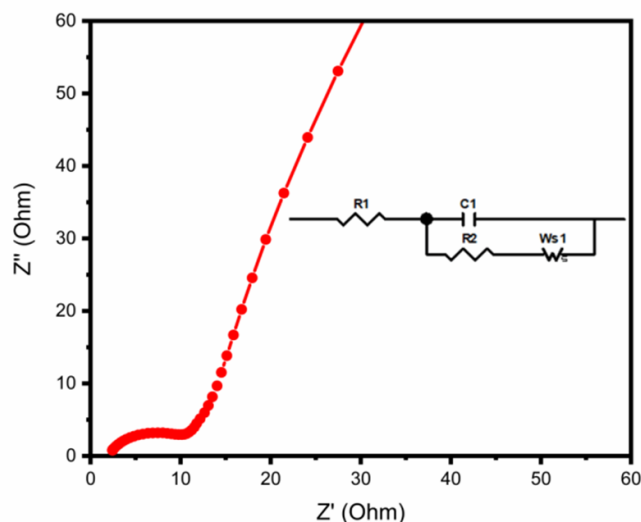

FIG. 11. The Nyquist plot of NiS powder electrode synthesized at 2 molar sulphur concentrations. Inset shows the electrical equivalent circuit used for the fitting impedance spectra.

4. Conclusion

We have successfully synthesized nickel sulfide nanoparticles using the simple and low-cost hot injection method in oleylamine solvent. The absorption spectrum of NiS nanoparticles is blue-shifted compared to bulk material, indicating the presence of small size of crystallites in the synthesized material. The optical band gap energy of NiS nanoparticles was found in the range of 1.81 to 1.98 eV. It shows that the synthesized NiS nanoparticles are suitable for energy conversion device applications. The X-ray diffraction pattern and the Raman spectra confirm the formation of high purity NiS nanoparticles. The samples synthesized at 2 molar sulphur concentrations have a good crystalline nature as compared with the other two samples. Thus, the crystallinity of the synthesized materials highly dependents on sulphur concentrations. The agglomeration of nanoparticles was observed from SEM images. The electrochemical studies show that synthesized NiS nanoparticles is a promising material for supercapacitor electrode applications. The estimated values of specific capacitance, energy density and power density are 315.8 F/g, 6.99 WhKg^{-1} and 199 Wkg^{-1}, respectively. In this work, 2 molar sulphur concentrations are optimized for the synthesis of superiority nanoparticles. The crystallinity, particle size, morphology and electrochemical performance of NiS nanoparticles strongly depend on sulphur concentration. Thus, the present study shows that sulphur concentration plays an important role in the synthesis of high-quality NiS nanoparticles. This work provides that the hot injection method is a novel method for the synthesis of device quality nickel sulfide and other metal sulfides for energy conversion and energy storage applications.

References

[1]   Wang G., Zhang L., Zhang J. A review of electrode materials for electrochemical supercapacitors. *Chem. Soc. Rev.*, 2012, **41**, P. 797–828.
[2]   Gao Y.P., Wu X., Huang K.J., Xing L.L., Zhang Y.Y., Liu L. Two-dimensional transition metal diseleniums for energy storage application: a review of recent developments. *Cryst. Eng. Comm.*, 2017, **19**, P. 404–418.
[3]   Parveen N., Ansari M.O., Ansari S.A., Cho M.H. Simultaneous sulfur doping and exfoliation of graphene from graphite using an electrochemical method for supercapacitor electrode materials. *J. Mater. Chem. A*, 2016, **4**, P. 233–240.
[4]   Zhang L.L., Zhao X.S. Carbon-based materials as supercapacitor electrodes. *Chem. Soc. Rev.*, 2009, **38**, P. 2520–2535.
[5]   De B., Balamurugan J., Kimand N.H., Lee J.H. Enhanced electrochemical and photocatalytic performance of core–shell CuS@ carbon quantum dots@ carbon hollow nanospheres. *ACS applied materials & interface*, 2017, **9** (3), P. 2459–2468.

[6] Guan B.Y., Yu L., Wang X., Song S., Lou X.W. Formation of Onion-Like $NiCo_2S_4$ Particles via Sequential Ion-Exchange for Hybrid Supercapacitors. *Adv. Mater.*, 2017, **29**, 1605051.

[7] Chen H., Jiang J., Zhang L., Xia D., Zhao Y., Guo D., Qi T., Wan H. In situ growth of NiCo2S4 nanotube arrays on Ni foam for supercapacitors: Maximizing utilization efficiency at high mass loading to achieve ultrahigh areal pseudocapacitance. *J. Power Sources*, 2014, **254**, P. 249–257.

[8] Zhang Z., Wang Q., Zhao C., Min S., Qian X. One-step hydrothermal synthesis of 3D petal-like $Co_9S_8/RGO/Ni_3S_2$ composite on nickel foam for high-performance supercapacitors. *ACS Appl. Mater. Inter.*, 2015, **7**, P. 4861–4868.

[9] Gou J., Xie S., Yang Z., Liu Y., Chen Y., Liu Y., Liu C. A high-performance supercapacitor electrode material based on NiS/Ni_3S_4 composite. *Electrochimi. Acta*, 2017, **229**, P. 299–305.

[10] Yang J., Duan X., Guo W., Li D., Zhang H., Zheng W. Electrochemical performances investigation of NiS/rGO composite as electrode material for supercapacitors. *Nano Energy*, 2014, **5**, P. 74–81.

[11] Wang P.T., Zhang X., Zhang J., Wan S., Guo S.J., Lu G., Yao J.L., Huang X.Q. Precise tuning in platinum-nickel/nickel sulfide interface nanowires for synergistic hydrogen evolution catalysis. *Nat. Commun.*, 2017, **8**, 14580.

[12] Ye C., Zhang L., Guo C.X., Li D.D., Vasileff A., Wang H.H., Qiao S.Z. A 3D Hybrid of chemically coupled nickel sulfide and hollow carbon spheres for high performance lithium-sulfur batteries. *Adv. Funct. Mater.*, 2017, **27** (33), 1702524.

[13] Sun H.C., Qin D., Huang S.Q., Guo X.Z., Li D.M., Luo Y.H., Meng Q.B. Dye-sensitized solar cells with NiS counter electrodes electrodeposited by a potential reversal technique. *Energy Environ. Sci.*, 2011, **4** (8), P. 2630–3637.

[14] Ajibade P.A., Nqombolo A. Synthesis and Structural Studies Of Nickel Sulphide And Palladium Sulphide Nanocrystals. *Chalcogenide Letters*, 2016, **13** (9), P. 427–434.

[15] Salavati-Niasari M., Banaiean-Monfared G., Emadi H., Enhessari M. Synthesis and characterization of nickel sulfide nanoparticles via cyclic microwave radiation. *Comptes Rendus Chimie*, 2013, **16** (10), P. 929–936.

[16] Karthikeyan R., Navaneethan M., Archana J., Thangaraju D., Arivanandhan M., Hayakawa Y. Shape controlled synthesis of hierarchical nickel sulfide by the hydrothermal method. *Dalton Trans.*, 2014, **43** (46), P. 17445–17452.

[17] Yang P., Song B., Zheng Y., Sun Y., Jian J.K. Solvothermal growth of NiS single-crystalline nanorods. *J. Ally Compd.*, 2009, **481**, P. 450–454.

[18] Peng L., Ji X., Wan H., Ruan Y., Xu K., Chen C., Miao L., Jiang J. Nickel Sulfide Nanoparticles Synthesized by Microwave-assisted Method as Promising Supercapacitor Electrodes: An Experimental and Computational Study. *Electrochimica Acta*, 2015, **182**, P. 361–367.

[19] Kristl M., Dojer B., Gyergyek S., Kristl J. Synthesis of nickel and cobalt sulfide nanoparticles using a low cost sonochemical method. *Heliyon*, 2017, **3** (3), e-00273-00292.

[20] Kamble M.M., Nasane M.P., Rondiya S.R., Dzade N.Y., Bade B.R., Funde A.M., Kore K.B., Jadkar S.R. Optical, structural and morphological study of CdS nanoparticles: role of sulfur source. *Nanomaterials and Energy*, 2020, **9** (1), P. 72–81.

[21] Karthikeyan R., Thangaraju D., Prakashand N., Hayakawa Y. Single-step synthesis and catalytic activity of structure-controlled nickel sulfide nanoparticles. *Cryst. Eng. Comm.*, 2015, **17**, P. 5431–5439.

[22] Bishop D.W., Thoms P.S., Ray A.S. Raman Spectra of Nickel(II) Sulfide. *Mater. Res. Bull.*, 1998, **33** (9), P. 1303–1306.

[23] Yoshikawa M., Murakami M., Matsuda K., Matsunobe T., Sugie S., Okada K., Ishida H. Characterization of Si nano-polycrystalline films at the nanometer level using resonant Raman scattering. *J. Appl. Phys.*, 2005, **98**, P. 63531–63533.

[24] Kamble M.M., Waman V.S., Maybadi A., Funde A.M., Sathe V.G., Shripati T., Pathan H.M., Jadkar S.R. Synthesis of cubic nanocrystalline silicon carbide (3C-SiC) films by HW-CVD method. *Silicon*, 2017, **9** (3), P. 421–429.

[25] Chen X.Y., Wang Z.H., Wang X., Wan J.X., Liu J.W., Qian Y.T. A single-source approach to metastable Ni_3S_4 crystallites and their optical properties. *Chem. Lett.*, 2004, **33** (10), P. 1294–1295.

[26] Hu Y.,Chen J.F., Chen W.M., Lin X.H., Li X.L. Synthesis of Novel Nickel Sulfide Submicrometer Hollow Spheres. *Adv. Mater.*, 2003, **15**, P. 726–729.

[27] Tauc J. (Ed.) *Amorphous and Liquid Semiconductor*, Plenum Press, New York, 1974, **159**.

[28] Yong Xu, Martin A.A. Schoonen. The absolute energy positions of conduction and valence bands of selected semiconducting minerals. *American Mineralogist*, 2000, **85**, P. 543–556.

[29] Darezereshki E., Vakylabad A.B., Hassanzadeh A., Niedoba T., Surowiak A., Koohestani B. Hydrometallurgical Synthesis of Nickel Nano-Sulfides from Spent Lithium-Ion Batteries. *Minerals*, 2021, **11**, P. 419–431.

[30] Bobinihi F.F., Fayemi O.E., Onwudiwe D.C. Synthesis, characterization, and cyclic voltammetry of nickel sulphide and nickel oxide nanoparticles obtained from Ni(II) dithiocarbamate. *Materials Science in Semiconductor Processing*, 2021, **121**, P. 105315–105327.

[31] Buchmaier C., Glanzer M., Torvisco A., Poelt P., Wewerka K., Kunert B., Gatterer K., Trimmel G., Rath T. Nickel sulfide thin films and nanocrystals synthesized from nickel xanthate precursors. *J. Mater Sci Electronic materials*, 2017, **52** (18), P. 1–17.

[32] Howatt G., Breckenridg R. Fabrication of Thin ceramic Sheets for Capacitors. *J. Brownlow, J. Am. Ceram. Soc.*, 1947, **30**, P. 237–242.

[33] Krebs F.C. Fabrication and processing of polymer solar cells: a review of printing and coating techniques. *Solar Energy Materials and Solar Cells*, 2009, **93**, P. 394–412.

[34] Emmenegger C., Mauron P., Sudan P., Wenger P., Hermann V., Gallay R., Zuttel A. Investigation of electrochemical double-layer (ECDL) capacitors electrodes based on carbon nanotubes and activated carbon materials. *J. Power Sources*, 2003, **124**, P. 321–329.

[35] Sylla N.F., Ndiaye N.M., Ngom B.D., Momodu D., Madito M.J., Mutuma B.K., Manyala N. Effect of porosity enhancing agents on the electrochemical performance of high-energy ultracapacitor electrodes derived from peanut shell waste. *Sci. Rep.*, 2019, **9** (2019), P. 13673–13688.

[36] Kumar Y.A., Rao S.S., Punnoose D., Tulasivarma C.V., Chandu V.V.M. Gopi, Prabakar K., Kim H.J. Influence of solvents in the preparation of cobalt sulfide for supercapacitors. *R. Soc. Open Sci.*, 2017, **4**, P. 170427–170438.

[37] Marand N.A., Masoudpanah S.M., Alamolhoda S., Bafghi M.Sh. Solution combustion synthesis of nickel sulfide/reduced graphene oxide composite powders as electrode materials for high-performance supercapacitors. *J. of Energy Storage*, 2021, **39**, P. 102637–102644.

[38] Meena S., Anantharaju K., Malini S., Dey A., Renuka L., Prashantha S., Vidya Y. Impact of temperature-induced oxygen vacancies in polyhedron $MnFe_2O_4$ nanoparticles: As excellent electrochemical sensor, supercapacitor and active photocatalyst. *Ceram. Int.*, 2021, **10**, P. 14723–14740.

[39] Manohar A., Vijayakanth V., Vattikuti S., Kim K.H. Structural and electrochemical properties of mixed calcium-zinc spinel ferrites nanoparticles. *Ceram. Int.*, 2022, **48** (20), P. 30695–33070.

Information about the authors:

Mahesh Mahadev Kamble – PDEA'S Anantrao Pawar College, Pirangut, Mulshi, Pune 412115 India; ORCID 0000-0001-6835-5674; mmkamble14@gmail.com

Bharat Rambhau Bade – Department of Physics, Savitribai Phule Pune University, Pune 411007 India; ORCID 0000-0001-8450-6807; badebharat94@gmail.com

Avinash Vinayak Rokade – Department of Physics, Savitribai Phule Pune University, Pune 411007 India; ORCID 0009-0002-3892-2580; avinashrokade12@gmail.com

Vaishali Sambhaji Waman – P. E. S. Modern College of Arts, Science and Commerce, Shivajinagar, Pune 411005 India; ORCID 0009-0003-1925-9637; vaishaliwaman@gmail.com

Sachin Vasant Bangale – Chemical Research Lab, UG and PG Department of Chemistry, G. M. Vedak College of Science, Tala-Raigad, 402111 India; ORCID 0000-0003-3495-7313; sachinbangale98@gmail.com

Sandesh Rohidas Jadkar – Department of Physics, Savitribai Phule Pune University, Pune 411007 India; ORCID 0000-0002-0610-7242; sandesh@physics.unipune.ac.in